Ocean Dynamics (2002) 52: 95–103
DOI 10.1007/s10236-001-0011-2

John L. Wilkin · Melissa M. Bowen · William J. Emery

Mapping mesoscale currents by optimal interpolation of satellite radiometer and altimeter data

Received: 3 July 2001 / Accepted: 16 November 2001

Abstract Mapping the mesoscale surface velocity stream function by combining estimates of surface height from satellite altimetry and surface currents from sequential infrared (sea-surface temperature) imagery using optimal interpolation is described. Surface currents are computed from infrared images by the method of maximum cross-correlations (MCC) and are combined with altimeter sea-level anomaly data from the TOPEX/Poseidon and ERS satellites. The analysis method was applied to 6 years of data from the East Australian Current region. The covariance of velocity and sea-level data is consistent with the statistical assumptions of homogeneous, isotropic turbulence, with typical length scales of order 220 km and time scales of 10 days in this region. Augmenting the analysis of altimeter data with MCC velocity observations improves the resolution of the surface currents, especially near the Australian coast, and demonstrates that the two data sources provide consistent and complementary observations of the surface mesoscale circulation. The volume of MCC data is comparable to that from a satellite altimeter, but with a more variable distribution of spatial and temporal resolution. In concert with altimetry, satellite radiometer velocimetry represents a technique useful for retrospective analysis of currents from high-resolution satellite radiometer data-sets.

Keywords Mesoscale currents · Optimal interpolation · Covariance scales · Altimeter · Radiometer · East Australian Current

Responsible Editor: Rosemary Morrow

J. L. Wilkin (✉)
Institute of Marine and Coastal Sciences,
Rutgers University, New Jersey, USA
e-mail: wilkin@imcs.rutgers.edu

J. L. Wilkin · M. M. Bowen
National Institute of Water and Atmospheric Research,
New Zealand

M. M. Bowen · W. J. Emery
University of Colorado, Boulder, USA

1 Introduction

Satellite thermal imagery from the advanced very high-resolution radiometer (AVHRR) instrument aboard the NOAA polar orbiting satellites has proven effective for visualizing the short space and time scales of ocean-surface variability in coastal and boundary current regions. However, utilizing these satellite observations to quantify mesoscale surface currents in shelf seas and the adjacent deep ocean has proven challenging.

In regions where sea-surface temperature gradients are representative of upper ocean density gradients, near-surface along-isotherm velocity has been inferred for individual satellite images by application of the thermal wind relation (Essen 1995; Strub et al. 1997). More widely applicable approaches utilize pairs of thermal images observed several hours apart, and assume the changes from one image to the next are predominantly due to advection (Emery et al. 1986).

Surface velocities can be inferred using inverse methods based on the temperature conservation equation (Kelly 1989; Kelly and Strub 1992; Vigan et al. 2000). These methods seek a velocity solution consistent with the evolution of the temperature field during the interval between satellite passes, making allowance for air–sea interaction and applying constraints to divergence, vorticity, and/or smoothness of the flow.

An alternative approach is to locate the maximum cross-correlation (MCC) in windowed portions of the image pairs. This objectively defines the displacement that has occurred between image times, and hence the velocity. This so-called MCC method has been applied to AVHRR imagery from the coast of British Columbia (Emery et al. 1986), the US West Coast (Tokmakian et al. 1990; Simpson and Gobat 1994), the Gulf Stream (Emery et al. 1992), and the Brazil-Malvinas Confluence (Domingues et al. 2000). A comparative study using the same set of image pairs showed that the inverse and MCC methods give similar agreement with in situ current observations (Kelly and Strub 1992). The MCC method is also applicable to visible imagery such as ocean color (Tokmakian et al. 1990).

Clouds obscure radiometer imagery of the ocean surface, and the above studies each considered only small sets of uncharacteristically clear image pairs to demonstrate the methods. The utility of radiometer observations for making long-term observations of mesoscale currents had not been proven until the MCC method was applied to several years of daily AVHRR imagery for the East Australian Current region by M. M. Bowen personal communication (2001), hereafter referred to as Bowen et al. (2001).

The advent of satellite altimetry has introduced a further method for observing the ocean mesoscale. An altimeter measures sea-level height along the satellite groundtrack, from which the component of velocity normal to the groundtrack may be computed by geostrophy. Comparison with in situ current observations indicates that an altimeter such as TOPEX/Poseidon (T/P) resolves horizontal scales of approximately 50 km in the along-track direction (Strub et al. 1997). Studies of mesoscale circulation typically map these along-track data to two-dimensional gridded height fields using optimal interpolation (Le Traon and Hernandez 1992; Hernandez et al. 1995; Le Traon et al. 1998) and then compute geostrophic currents. Alternative space–time interpolation methods such as spline function fitting (Mesias and Strub 1995; Brankart and Brasseur 1996) give comparable results.

The 250 km or so that separate T/P groundtracks, and the 10 days between repeat passes, mean that the dense along-track resolution cannot be realized throughout a gridded dataset. Incorporating data from another altimeter satellite in a complementary orbit, such as the European Space Agency ERS satellites, significantly improves resolution (Hernandez et al. 1995), yet calculations of how many satellites are required to form an ocean-observing system capable of resolving the mesoscale indicate that a minimum of two, and preferably four or more, altimeters are required (Le Traon et al. 1999).

Shortcomings in the accuracy of geoid estimates at short wavelengths, especially in boundary current regions, means that altimeters do not reliably observe the mean sea level in the EAC. Consequently, the long-term mean is generally removed from altimeter observations and analysis limited to consideration of the sea-level anomaly. In contrast, Bowen et al. (2001) found that the MCC method resolves persistent coastal currents quite well. A further distinction in the datasets is that altimetry reveals geostrophic flow only, whereas MCC data are interpreted as a total velocity that may include ageostrophic processes that advect thermal patterns.

It is attractive, therefore, to be able to combine velocity information from radiometers and altimeters in a manner that will allow the respective sampling distributions, and type of observation, of the two instruments to complement each other.

Covariance scales and error characteristics of the MCC velocity data and altimeter data in the East Australian Current are described in Section 2, and the optimal interpolation scheme in Section 3. The results (Sect. 4) show examples of East Australian Current surface velocity stream function illustrating that the altimeter and MCC data are consistent and that the sampling patterns of the two are complementary. Section 5 summarizes the results, concluding that merging the two datasets reduces expected errors in the stream function mapping and improves the resolution of mesoscale circulation.

2 Data

2.1 Altimeter data

The altimeter data we use are derived from the T/P and ERS-2 Geophysical Data Records by applying standard environmental corrections (wet and dry troposphere correction, ionosphere correction, sea-state bias, solid earth tides and pole tides, the CSR ocean tide correction, and the inverse barometer effect) (AVISO/Altimetry 1996). After removing the long-term mean (to remove any signal from an imprecisely known geoid), the sea-level anomaly data were filtered along track with a ten-point boxcar filter to reduce instrument noise, and decimated by a factor of 10 to return largely independent observations at 0.5° (T/P) or 0.6° (ERS-2) latitude (approximately 60-km) intervals.

2.2 MCC velocity data

To date, studies that calculate velocities from radiometer image sequences have tended to concentrate on development and validation of the methods. Satellite radiometer velocimetry had not been applied to a long image time series until Bowen et al. (2001) analyzed data archived from the high-resolution picture transmission (HRPT) receiver at the CSIRO Marine Laboratories in Hobart, Tasmania, Australia. Data archived from the AVHRR instrument on the NOAA-9, 12, 14, and 15 satellites for the 6 years 1993–1998 comprise over 20 000 images of the East Australian Current (EAC).

In any application of the MCC algorithm, certain parameters must be set. These include the size of the image subset window that is searched for an apparent displacement, the range of time separations between images that yields useful results, a cutoff value for the cross-correlation coefficient that represents a valid displacement vector, and consistency checks for neighboring vectors that will reduce the occurrence of spurious data. Bowen et al. (2001) tested the sensitivity of the MCC method with a large subset of the EAC data, plus imagery from the California Current, identifying a set of MCC parameters that give robust results. Computing MCC vectors on a 15-km grid, using 30-km image subsets and all available image pairs with a separation of

3 to 13 h, the EAC images yielded, on average, 8000 vectors in a 30-day period despite clouds rendering large areas of many images unusable.

Valid MCC vectors are often registered at the same location for several consecutive days during an extended period of clear skies and, as a result, the volume of MCC data is substantial. This is problematic for optimal interpolation because of the consequent size of the matrix computations required. We therefore reduce the MCC data by taking 3-day, 30-km composites. The temporal average is justified by noting that mesoscale currents are strongly autocorrelated over a few days' time scale, and hence daily MCC vectors are not strictly independent. The 30-km average is warranted because, by searching 30-km image subsets at 15-km intervals, adjacent vectors are not independent. The compositing step also has the advantage of reducing some of the data noise without appreciably sacrificing time or spatial resolution.

The final data density was typically 380 vectors every 10 days in the EAC domain (Fig. 1), at a spatial resolution of nominally 30 km. Ten-day periods with fewer than 200 vectors occur less than 20% of the time. T/P and ERS-2 combined return 300 along-track height observations in 10 days. Arguably, the MCC method is therefore capable of observing mesoscale currents at a resolution comparable to two satellite altimeters.

The composited MCC velocity data, and the filtered, decimated T/P and ERS-2 along-track sea-level anomaly data, comprise the set of observations that we combine by optimal interpolation to map the surface velocity stream function.

3 Analysis methods

3.1 Optimal interpolation

Optimal interpolation (OI) (also referred to as objective analysis) was introduced to oceanography by Bretherton et al. (1976) and has been described further by, e.g., McIntosh (1990) and Le Traon et al. (1999). OI makes an estimate of a variable, say $\psi(x)$, from a weighted linear combination of observations ϕ_i^{obs} made at irregular locations x_i (in space and time). The weights are chosen so that the estimate has the minimum expected ensemble mean squared error. The data need not be of uniform type, provided ψ and the data are linearly related (McIntosh 1990). The vector of optimal estimates at a set of grid locations x is given by

$$\psi^{\mathrm{est}}(x) = \mathbf{C}\mathbf{A}^{-1}\phi^{\mathrm{obs}} \tag{1}$$

where matrix $\mathbf{C}$ is the covariance of the variable being estimated with the data:

$$C_{ij} = \langle \psi_i^{\mathrm{est}} \phi_j^{\mathrm{obs}} \rangle = \langle \psi_i^{\mathrm{est}} \phi_j \rangle$$

and $\mathbf{A}$ is the covariance of the data with each other:

$$A_{ij} = \langle \phi_i^{\mathrm{obs}} \phi_j^{\mathrm{obs}} \rangle = \langle \phi_i \phi_j \rangle + \langle e_i e_j \rangle \tag{2}$$

Here, $\phi_i^{\mathrm{obs}} = \phi_i + e_i$, where ϕ_i is the true value and e_i is the measurement error. If the e_i are uncorrelated, the noise covariance matrix $\langle e_i e_j \rangle$ is simply $e^2 \delta_{ij}$.

The square of the expected error in the estimate at location x_k is:

$$E^2(x_k) = s_\psi^2 - \mathbf{c}_k \mathbf{A}^{-1} \mathbf{c}_k^T \tag{3}$$

where s_ψ^2 is the variance of ψ, and $\mathbf{c}_k$ is the covariance of $\psi^{\mathrm{est}}(x_k)$ with the data; namely, the k^{th} row of $\mathbf{C}$.

We choose to map surface velocity stream function from the MCC and altimeter data in a manner similar to previous analyses of drifter velocities (McWilliams 1976; Le Traon and Hernandez 1992), shipboard acoustic Doppler current profiler (ADCP) data (Walstad et al. 1991; Chereskin and Trunnell 1996), and MCC data (Kelly and Strub 1992). The principal argument for mapping to a stream function is that mesoscale circulation is strongly geostrophic and hence weakly divergent. Mapping to a nondivergent stream function serves to largely filter out ageostrophic components of flow in the direct observations of velocity. This is particularly desirable in our application because we combine MCC velocity with altimetry, from which only the geostrophic component of velocity can be inferred.

For homogeneous, isotropic turbulence, velocity covariances are related to stream-function covariance $C_{\psi\psi}(r)$ by (Bretherton et al. 1976; Le Traon and Hernandez 1992)

$$\begin{aligned}
C_{uu} &= \frac{x^2}{r^2}(R - S) + S \\
C_{vv} &= \frac{y^2}{r^2}(R - S) + S \\
C_{uv} &= \frac{xy}{r^2}(R - S) \\
C_{\psi u} &= yR \\
C_{\psi v} &= -xR \ ,
\end{aligned} \tag{4}$$

where $r = (x^2 + y^2)^{1/2}$ is the spatial separation, and

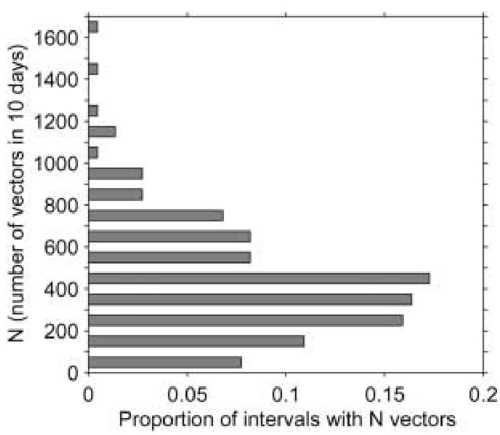

Fig. 1 Histogram of the number of MCC vectors every 10 days during 1993–1998. The median is 380. The combination of T/P and ERS returns 300 observations every 10 days

$$R = -\frac{1}{r}\frac{\mathrm{d}C_{\psi\psi}}{\mathrm{d}r}, \quad S = -\frac{\mathrm{d}^2 C_{\psi\psi}}{\mathrm{d}r^2} \quad . \tag{5}$$

If the velocity is geostrophic, then ψ and sea-level anomaly, h, are proportional with a factor f, the local Coriolis parameter, divided by g, the gravitational acceleration. Covariances involving h are then $C_{hh} = (f/g)^2 C_{\psi\psi}$, $C_{hu} = (f/g)C_{\psi u}$, and $C_{hv} = (f/g)C_{\psi v}$.

To implement the multivariable OI, the covariance matrices **C** and **A** in Eq. (1) are formulated thus:

$$\mathbf{A} = \begin{bmatrix} \mathbf{C}_{uu} + e_u^2\mathbf{I} & \mathbf{C}_{uv} & \mathbf{C}_{uh} \\ \mathbf{C}_{uv} & \mathbf{C}_{vv} + e_u^2\mathbf{I} & \mathbf{C}_{vh} \\ \mathbf{C}_{uh} & \mathbf{C}_{vh} & \mathbf{C}_{hh} + e_h^2\mathbf{I} \end{bmatrix}$$

$$\mathbf{C} = \left[\mathbf{C}_{\psi u}\mathbf{C}_{\psi v}\mathbf{C}_{\psi h}\right] \quad ,$$

where e_u^2 and e_h^2 are the noise variance of the MCC and altimeter observations, respectively, and **I** is the identity matrix. The data vector is a concatenation of the available observations:

$$\phi^{\mathrm{obs}} = \begin{bmatrix} \mathbf{u}^{mcc} \\ \mathbf{v}^{mcc} \\ \mathbf{h}^{alt} \end{bmatrix}$$

3.2 Data covariance scales and error variance

The velocity (Fig. 2) and sea-level anomaly (Fig. 3) spatial covariance were estimated by computing data covariance values at zero time lag, binned according to spatial lag, and averaging over the 6 years of data. To these data we fit functions derived according to Eqs. (4) and (5) from the spatial covariance structure

$$C_{\psi\psi}(r) = s_\psi^2\left[1 + ar + \tfrac{1}{6}(ar)^2 - \tfrac{1}{6}(ar)^3\right]e^{-ar} \tag{6}$$

used by Le Traon and Hernandez (1992) to map, separately, mesoscale altimeter and drifter data. The correct x–y asymmetry in C_{uu}, C_{uv}, and C_{vv} evident in Fig. 2 indicates that the homogeneous, isotropic turbulence model adequately represents the observed velocity variability.

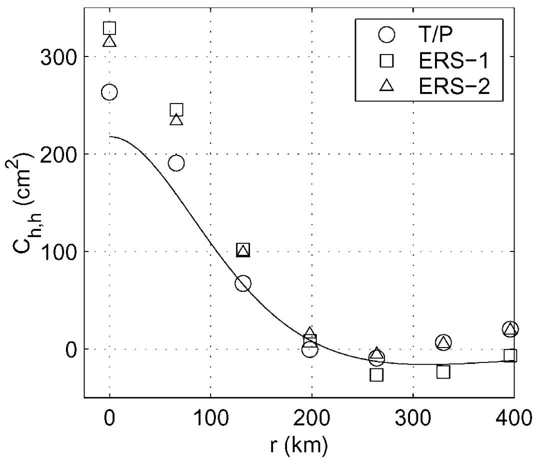

Fig. 3 Covariance of along-track sea-level anomaly C_{hh} at zero time lag. Data values binned according to spatial lag r for TOPEX/Poseidon (◯), ERS-1 (□), and ERS-2 (△), and Eq. (6) fitted to the data ($1/a$ = 65 km) (*solid line*). *Units* are cm^2

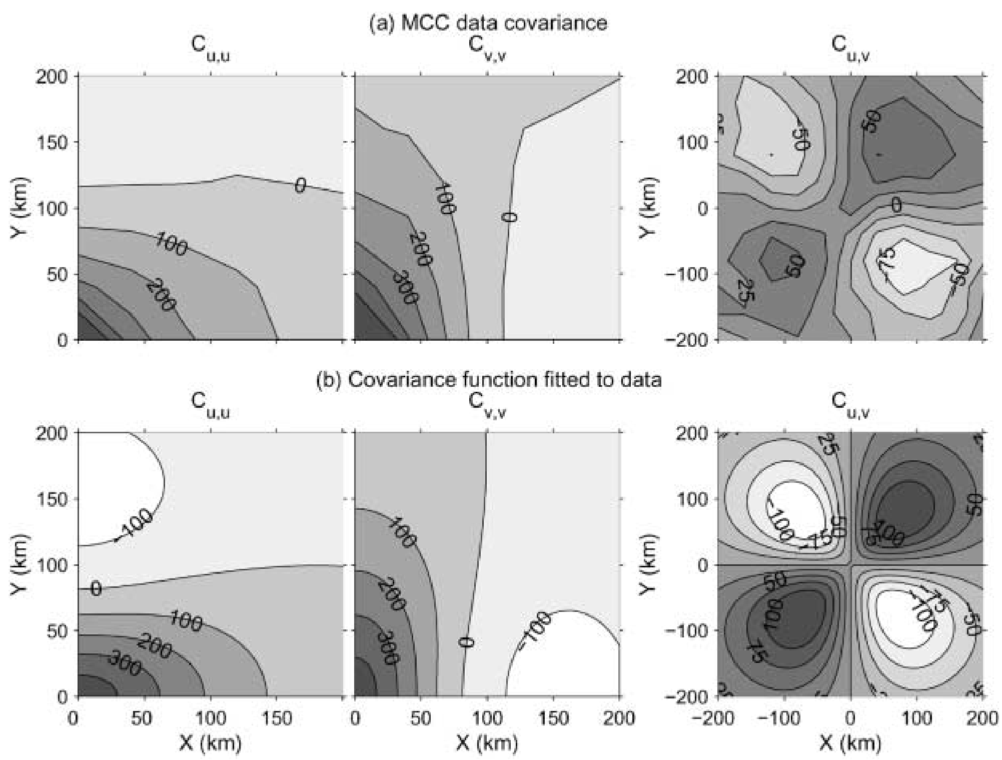

Fig. 2 **a** Covariance of MCC velocity C_{uu}, C_{vv}, and C_{uv}, at zero time lag, binned according to spatial lag X and Y and averaged over years 1993–1998. **b** The covariance function of Eq. (6) fitted to the data ($1/a$ = 65 km). *Units* are cm^2 s^{-2}

The isotropic turbulence model defines the signal variances at zero lag (s_u^2, s_h^2) in terms of s_ψ^2, and it follows from Eq. (6) that the ratio $s_h^2/s_u^2|_{r=0} = 3f^2/(2a^2g^2)$. Fitting Eq. (6) to the data therefore implies that the length scales and signal variance of both velocity and sea-level anomalies can be fit with a single choice of parameter a. The values $1/a = 65$ km and $s_u^2 = 450$ cm^2 s^{-2} fit the velocity data well (Fig. 2). These values imply a sea-level anomaly variance, at zero lag, of around 220 cm^2, which is lower than the 280 cm^2 we observe for T/P data. Increasing $1/a$ to better fit s_h^2 would cause a drop off with r that is too gradual and risks the OI placing undue weight on data that is distant from the estimation location. The chosen length scale is a compromise to fitting both data types, with the possible result of somewhat underestimating the signal variance of the altimeter data.

The scale $1/a = 65$ km corresponds to a zero crossing in the stream-function covariance at $r = 220$ km. This is greater than typically used to map mesoscale observations from altimetry or drifters (e.g., $1/a$ =40–45 km, Le Traon Hernandez 1992; Le Traon et al. 1999).

The spatial covariance function was augmented with time dependence $\exp -t/T$ ($T = 10$ days). This fits the observed MCC temporal covariance better than a Gaussian function (Fig. 4), and is similar to the observed covariance of mesoscale sea-surface temperature in the EAC region (Walker and Wilkin 1998). The temporal covariance was estimated only for MCC data because there are few altimeter groundtrack cross-overs at lags of less than 5 days, making it difficult to resolve the mesoscale covariance time scale.

Examining the data covariance also provides a measure of the observational error. For uncorrelated errors, the data covariance at zero lag is the signal variance plus a delta peak due to the independent error variance (Eq. 2). Figure 4 suggests that errors in the MCC velocity are approximately $e_u = 0.20$ m s^{-1}, which is the upper limit of error values determined by Bowen et al. (2001).

We assume an altimeter height error of $e_h = 0.03$ m following Strub et al. (1997), who considered errors in cross-track velocity calculated from T/P data that were processed in a manner similar to ours. We adopt this value for both the T/P and ERS data, though sensitivity tests show that this is not a critical choice.

4 Results

Sea-level anomaly data and anomaly velocities (6-year MCC mean removed) for 1993–1998 were mapped to anomaly stream function using the OI parameters selected in Section 3. We present results here in terms of stream function ψ scaled by f/g to give equivalent sea-level anomaly. The 6-year MCC mean currents will be restored when we discuss verification in comparison to other velocity observations.

To illustrate the two datasets, Fig. 5 shows data in the 10 days centered on 30 May, 1998. There are 360 MCC vectors, which is close to the median for a 10-day interval. For comparison, the altimeter data are displayed as cross-track vectors of geostrophic velocity. The component of MCC velocity normal to altimeter

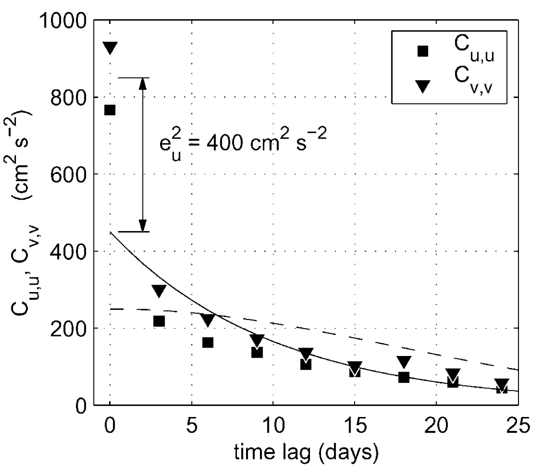

Fig. 4 Temporal covariance of velocity data at zero spatial lag, averaged over years 1993–1998. C_{uu} (■), C_{vv} (▼), and time dependence $\exp -t/T$ ($T = 10$ days) used in the OI covariance function (*solid line*). A Gaussian function such as $\exp -(t/20)^2$ (*dashed line*), often used for altimetry OI (e.g., Le Traon et al. 1999), is not consistent with these data. The jump at zero time lag indicates that an average estimate of the error appropriate for both velocity components is $e_u = 0.2$ m s^{-1}

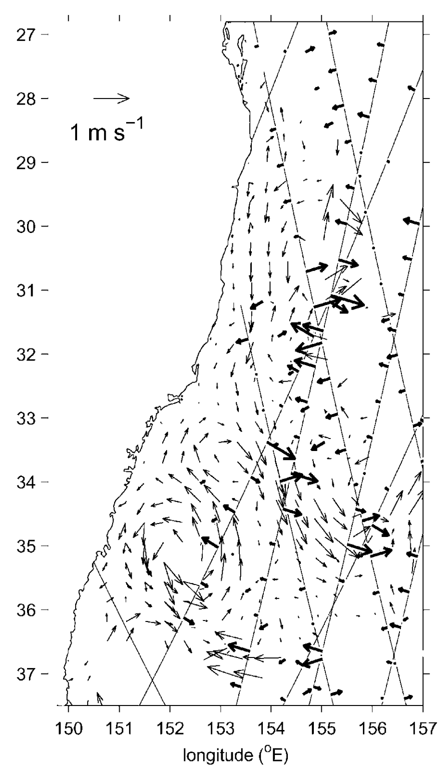

Fig. 5 Data for the 10-day interval centered on 30 May, 1998: MCC velocity (*light vectors*) and cross-track velocity from alitmetry (*dark vectors*) along altimeter groundtrucks (*light lines*)

tracks is in good agreement with neighboring estimates from sea level. This qualitative consistency is a general feature of the whole dataset. Both datasets capture the separated EAC jet flowing south and east from 34°S, 154°E to 35°S, 156°E. An anticyclone centered near 35°S, 152°E is resolved well by the MCC and also clipped by a T/P groundtrack.

When the MCC and altimeter data of Fig. 5 are optimally interpolated separately (Fig. 6a, b), different oceanographic features are resolved. On its own, altimetry captures the anticylonic flow centered at 34°S, 156°E that comprises the EAC separation and partial recirculation, and also significant eastward flow at 31°S. In the MCC map these flows are less intense, but the detached anticyclone at 35°S, 152°E is featured clearly. MCC streamlines show less tendency than altimetry to indicate flow normal to the coast. The joint mapping incorporates features resolved by both datasets (Fig. 6c). Along the coast, and where data fall between altimeter groundtracks (e.g., the anticyclone at 35°S, 152°E), the incorporation of MCC data introduces noticeable changes in the mapping.

Expected errors in ψ (Fig. 7) quantify the influence of data distribution on the analyses of 30 May, 1998. A cycle of T/P data is completed within the 10-day scale of stream-function covariance, and the T/P groundtrack pattern is clearly evident in Fig. 7a. ERS altimetry reduces the error along groundtracks transitted close to the analysis date. South of the region depicted in Figs. 5 and 6 there were few MCC data on this date, and expected errors there are correspondingly high. Figure 7d shows the extent to which the expected error in the altimeter-data-only mapping is reduced by the inclusion of MCC data. Where the error was already low due to recent T/P data, such as along the groundtrack that crosses the figure diagonally parallel to the coast, MCC offers modest improvement. However, further east and also along the coast, there is significant error reduction.

The long-term mean of expected errors (Fig. 8) quantifies how MCC data enhance the resolution of

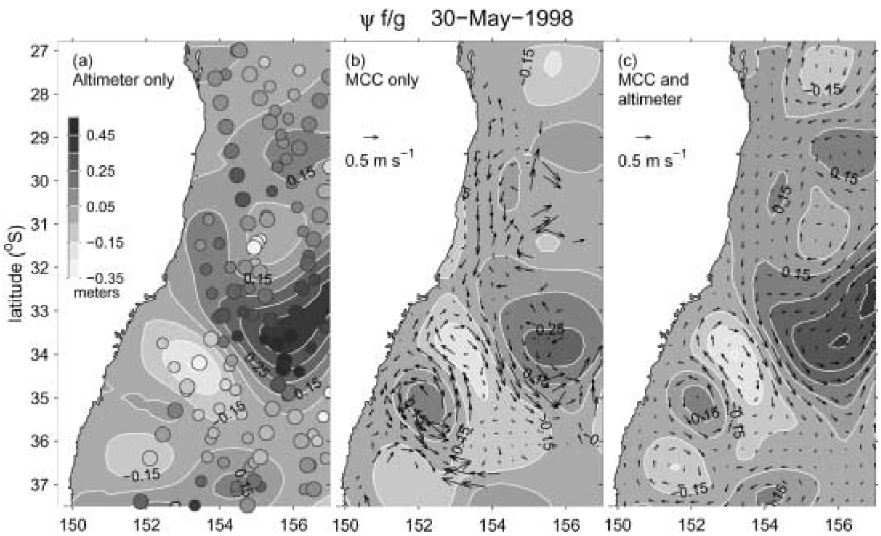

Fig. 6a–c Equivalent sea-level anomaly, $\psi f/g$ (meters), for 30 May, 1998, by optimal interpolation of **a** altimeter data only, **b** MCC data only, and **c** all data combined. Contour interval is 0.1 m and the *scale* in **a** applies to all panels. *Circles* in **a** show sea-level data with *shading* as for the underlying map and size indicating time lag to map date (large <5 days, small 5–10 days). Vectors in **b** are the MCC data (±5 days), and in **c** the velocity calculated from ψ

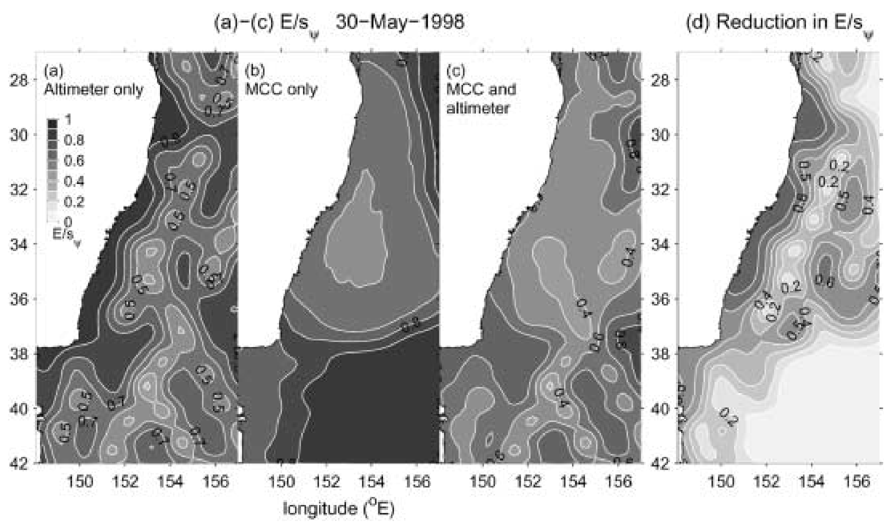

Fig. 7a–d Normalized expected error (E/s_ψ) from Eq. (3) for 30 May, 1998; **a–c** correspond to Fig. 6. **d** is the difference between **a** and **c** indicating where MCC data produce an improvement over altimetry alone. *Contour interval* is 0.1 and the *scale* in **a** applies to all panels

altimeter-only mesoscale maps. Throughout the EAC region, and especially within 200 km of the coast, there is a significant reduction in the expected errors of the OI due to incorporating MCC data.

4.1 Comparison to in situ data

A limited set of 17 drifters, deployed as part of the World Ocean Circulation Experiment Surface Velocity Program, traversed the EAC region between July 1995 and April 1997. The correlation between velocity observations from these drifters (Hansen and Poulain 1996) and the satellite analyses is given in Table 1. The correlation with velocities mapped from T/P alone is good, and moderately increases with the inclusion of ERS data. The subsequent addition of MCC data does not significantly improve the two-altimeter result. However, if the comparison is restricted to observations for which the corresponding satellite analysis has a low expected error ($E/s_\psi < 0.5$), then the influence of including additional data is more pronounced. The reason for this is apparent when the correlation calculation is made only for points where the addition of MCC data brings about a clear reduction in expected error (e.g., > 0.4 in Fig. 7d). In this case, the correlation coefficient increases markedly with the addition of MCC data. When altimeter data are absent, but MCC data are present, incorporating MCC data improves the correlation of drifter observations with the satellite analysis.

The drifter data comprise 305 days of 6-hourly kriged velocity observations (1220 data points), while restricting the comparison to results with reduced expected error halves this number. Given the 10-day time scale of variability, these data therefore have about 30 and 15 degrees of freedom, respectively, for which the tabulated correlations are all significant at the 95% confidence level. While the trends we observe in the correlation coefficients indicate a constructive role for the inclusion of MCC data, the available in situ drifter observations are few. The correspondingly low degrees of freedom lead to large error bounds on $|r|$ (Emery and Thompson 1998, Sect. 3.14.1) and the tabulated correlation coefficients are not significantly different from each other at the 95% level.

4.2 Residuals

The residuals of optimally interpolated fields should be consistent with the assumed error variance of the data. Examining the root mean squared difference of mapped velocities and MCC data, we find RMS residuals in the u and v components of 0.21 and 0.24 m s^{-1}, respectively, which are close to the assumed e_u of 0.2 m s^{-1}. The

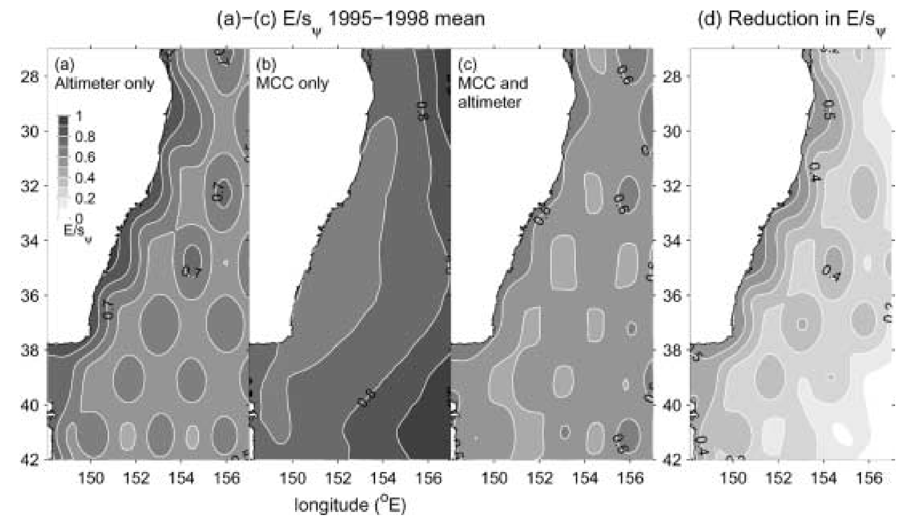

Fig. 8a–d Normalized expected error, as in Fig. 7, averaged over 1995–1998. *Contour interval* is 0.1 and the *scale* in **a** applies to all panels

Table 1 Correlation between surface drifter velocity and optimally interpolated satellite data

Data used in OI	Magnitude of complex correlation coefficient[a] $\|r\|$		
	All observations	$E/s_\psi < 0.5$[b]	Error reduction > 0.4[c]
T/P only	0.711	0.743	0.577
T/P + ERS	0.770	0.787	0.579
T/P + ERS + MCC	0.773	0.804	0.636

[a] r is computed for complex velocity $\mathbf{u} = u + iv$; $r = \mathrm{cov}(\mathbf{u}_1, \mathbf{u}_2)/[\mathrm{var}(\mathbf{u}_1)\mathrm{var}(\mathbf{u}_2)]^{1/2}$
[b] Calculated for points where case T/P + ERS + MCC has normalized expected error less than 0.5
[c] Calculated for points where including MCC data reduces expected error by more than 0.4

RMS residuals in sea-level anomaly are larger, averaging 6.5 cm, or double the assumed error of 3 cm.

The residual currents do not show coherent patterns that would indicate that the MCC data resolve significant ageostrophic flows missed by altimetry. There has not, therefore, been a significant loss of information by formulating the mapping procedure in terms of a velocity stream function.

We do not consider high altimeter residuals as evidence of MCC and altimeter giving contradictory observations. Indeed, an OI of altimeter data alone shows only slightly lower RMS residuals of 5.7 cm. This is more likely a consequence of the compromise made in fitting the covariance function to both datasets (Sect. 3.2).

The somewhat long (compared to other studies) covariance scale of $1/a = 65$ km may overly smooth the altimeter data, relegating to the residuals short-wavelength coherent signals observed by altimetry. To be consistent with a shorter covariance scale, the MCC data would need to show greater energy at short lags. Underestimation at short wavelengths could simply be a result of the 3-day, 30-km compositing step applied to reduce the MCC data volume. Reconciling the covariances of the two datasets might be easier if the MCC compositing criterion were relaxed to retain more energy at short scales.

5 Discussion and summary

The combination of MCC and altimetry has been attempted previously only by Kelly and Strub (1992). Their results were discouraging, showing that the addition of Geosat altimeter data to MCC vectors significantly degraded the MCC-only solution in a comparison with in situ velocity observations. However, their analysis was limited to data from only 3 days, and the accuracy of Geosat does not match that of T/P and ERS. The 6 years of East Australia Current MCC data (Bowen et al. 2001) used here offer a long time series suitable for assessing the utility of satellite radiometer velocimetry for monitoring surface current variability in a boundary current region.

The availability of vector observations rather than solely sea level, and the intermittently dense space (15 km) and time (1 day) sampling of the MCC data, made it possible to compute the covariance of mesoscale velocity over a wide range of spatial and temporal lags. We verified that a homogeneous, isotropic turbulence model adequately represents variability in this region.

Fitting the data covariance to the function proposed by Le Traon Hernandez (1992) showed that length scales in the EAC are greater than typically assumed for mid-latitude open-ocean regions. This is qualitatively consistent with the rather large anticyclones known to be shed regularly in the region (Nilsson and Cresswell 1981). Gaussian time covariance dependence is not a good model for variability in this region. This has not previously been apparent from studies of altimeter data because of limited availability of very short time lag observation pairs at groundtrack cross-over points. An exponential form was adopted that is also similar to temporal covariance in sea-surface temperature.

MCC and altimetry were found to give consistent estimates of the flow, indicating that the surface velocity from MCC is tracking the predominantly geostrophic currents. Optimally interpolating MCC and altimetry to surface velocity stream function can therefore take advantage of the different sampling distributions of the two datasets to produce a better-resolved mapping of surface currents.

Optimal interpolation provides objective estimates of expected errors in the results based on the assumed statistics of the data. In the EAC region, the addition of MCC data significantly reduces the expected error in mesoscale current maps compared to the analyses from two altimeters. A comparison of results with the limited set of in situ velocity observations in the region confirms that the greatest improvement in the correlation between drifter data and the satellite analysis occurs where the reduction in OI-expected error is greatest.

An unresolved issue raised by examining residuals of the OI is whether the preprocessing steps undertaken prior to mapping might have removed MCC energy at short-length scales. This could account for the difficulty in reconciling the signal variance of MCC and altimeter data at zero lag with a single covariance length scale. While expected error estimates from OI are sensitive to overestimation of the covariance scales (McIntosh 1990), we found relatively little sensitivity of the stream function results themselves to length scale and have not revisited the MCC compositing step. If more in situ data were available to validate the mapped velocities and their associated error estimates, we could better determine appropriate preprocessing steps to reduce the MCC data volume while retaining resolved mesoscale variability.

As an aside, we note that in a region with dense in situ observations from drifters, current meters, and shipboard ADCP (e.g., the California Current, Chereskin and Trunnell 1996; Miller et al. 1999), the present OI approach could be used to merge all available data, including satellite MCC and/or altimetry, to produce a highly resolved surface velocity stream-function analysis.

To use MCC data in studies of oceanic processes requires a long archive of well-navigated HRPT radiometer data. Many such datasets exist from ground stations worldwide, in some instances predating the launch of TOPEX/Poseidon. While cloudiness that plagues the application of sea-surface thermal imagery to oceanic studies remains a difficulty for compiling MCC observations, we have shown that the volume of MCC data can still rival that of a satellite altimeter.

MCC intermittently achieves higher resolution than altimetry, and the tendency for there to be more observations near the coast, where thermal gradients are pronounced, complements altimeter sampling by offering vector observations important for capturing the kinematics of flow in a boundary current; notably, improving the alignment of mapped streamlines with the coast.

The MCC analysis of satellite radiometry is a viable dataset for observing mesoscale surface currents. The data complement altimetry and represent a technique useful for retrospective analysis of historical HRPT datasets.

Acknowledgements This work was supported NASA's TOPEX/Poseidon/Jason program and the New Zealand Foundation for Research Science and Technology. The authors thank Australia's CSIRO Division of Marine Research for providing AVHRR data and access to AVISO altimeter data. We thank P. Sutton for helpful comments on a draft of the manuscript.

References

AVISO/Altimetry, AVISO user handbook for merged TOPEX/Poseidon products (1996) AVI-NT-02-101, ed 3.0

Brankart J-M, Brasseur P (1996) Optimal analysis of in situ data in the Western Mediterranean using statistics and cross-validation. J Atmos Ocean Technol 13: 477–491

Bretherton FP, Davis RE, Fandry CB (1976) A technique for objective analysis and design of oceanographic experiments applied to MODE-73. Deep Sea Res 23: 559–582

Chereskin TK, Trunnell M (1996) Correlation scales, objective mapping, and absolute geostrophic flow in the California Current. J Geophys Res 101: 22 619–22 629

Domingues CM, Gonçalves GA, Ghisolfi RD, Garcia CAE (2000) Advective surface velocities derived from sequential infrared images in the southwestern Atlantic Ocean. Remote Sensing Envir 73: 218–226

Emery WJ, Thompson RE (1998) Data analysis methods in physical oceanography. Pergamon, New York, 634 pp

Emery W, Thomas AC, Collins MJ, Crawford WR, Mackas DL (1986) An objective method for computing advective surface velocities from sequential infrared satellite images. J Geophys Res 91: 12 865–12 878

Emery WJ, Fowler C, Clayson CA (1992) Satellite-image-derived Gulf Stream currents compared with numerical model results. J Atmos Ocean Technol 9: 286–304

Essen H-H (1995) Geostrophic surface currents as derived from satellite SST images and measured by a land-based HF radar. Int J Remote Sensing 16: 239–256

Hansen DV, Poulain P-M (1996) Quality control and interpolations of WOCE/TOGA drifter data. J Atmos Ocean Technol 13: 900–909

Hernandez F, Le Traon P-Y, Morrow R (1995) Mapping mesoscale variability of the Azores Current using TOPEX/Poseidon and ERS 1 altimetry, together with hydrographic and Lagrangian measurements. J Geophys Res 100: 24 995–25 006

Kelly KA (1989) An inverse model for near-surface velocity from infrared images. J Phys Oceanogr 19: 1845–1864

Kelly KA, Strub PT (1992) Comparison of velocity estimates from advanced very high-resolution radiometer in the coastal transition zone. J Geophys Res 97: 9653–9668

Le Traon P-Y, Hernandez F (1992) Mapping the oceanic mesoscale circulation: validation of satellite altimetry using surface drifters. J Atmos Ocean Technol 9: 687–698

Le Traon P-Y, Nadal F, Ducet N (1998) An improved mapping method of multisatellite altimeter data. J Atmos Ocean Technol 15: 522–534

Le Traon P-Y, Dibarboure G, Ducet N (1999) How many altimeters are needed to map the ocean mesoscale circulation? In: Smith NR, Koblinsky C (Eds.) TOPEX/Poseidon Scientific Working Team Meeting Abstracts, San Raphaël, France, October 25–27

McIntosh PC (1990) Oceanographic data interpolation: objective analysis and splines. J Geophys Res 95: 13 259–13 541

McWilliams JC (1976) Maps from the mid-ocean dynamics experiment: part I. Geostrophic streamfunction. J Phys Oceanogr 6: 810–827

Mesias JM, Strub PT (1995) An inversion method to determine ocean surface currents using irregularly sampled satellite altimetry data. J Atmos Ocean Technol 12: 830–849

Miller AJ, McWilliams JC, Schneider N et al. (1999) Observing and modeling the California Current system. Eos Trans AGU 80: 533

Nilsson CS, Cresswell GR (1981) The formation and evolution of East Australian Current warm-core eddies. Prog Oceanogr 9: 133–183

Simpson JJ, Gobat JI (1994) Robust velocity estimates, stream functions and simulated Lagrangian drifters from sequential spacecraft data. IEEE Trans Geosci Remote Sensing 32: 479–493

Strub PT, Chereskin TK, Niiler PP, James C, Levine MD (1997) Altimeter-derived variability of surface velocities in the California Current System 1. Evaluation of TOPEX altimeter velocity resolution. J Geophys Res 102: 12 727–12 748

Tokmakian R, Strub PT, McClean-Padman J (1990) Evaluation of the maximum cross-correlation method of estimating sea-surface velocities from sequential satellite images. J Atmos Ocean Technol 7: 852–865

Vigan X, Provost C, Podesta G (2000) Sea-surface velocities from sea-surface temperature image sequences 2. Application to the Brazil-Malvinas confluence area. J Geophys Res 105: 19 515–19 534

Walker AE, Wilkin JL (1998) Optimal averaging of NOAA/NASA Pathfinder satellite sea-surface temperature data. J Geophys Res 103: 12 869–12 883

Walstad LJ, Allen JS, Kosro PM, Huyer A (1991) Dynamics of the coastal transition zone through data assimilation studies. J Geophys Res 96: 14 959–14 977